Eur. Phys. J. C (2018) 78:427
https://doi.org/10.1140/epjc/s10052-018-5924-8

THE EUROPEAN PHYSICAL JOURNAL C

Regular Article - Theoretical Physics

Monte Carlo Glauber model with meson cloud: predictions for 5.44 TeV Xe + Xe collisions

B. G. Zakharov[a]

L.D. Landau Institute for Theoretical Physics, GSP-1, 117940, Kosygina Str. 2, 117334 Moscow, Russia

Received: 15 April 2018 / Accepted: 19 May 2018 / Published online: 29 May 2018

Abstract We study, within the Monte-Carlo Glauber model, centrality dependence of the midrapidity charged multiplicity density $dN_{ch}/d\eta$ and of the anisotropy coefficients $\varepsilon_{2,3}$ in Pb + Pb collisions at $\sqrt{s} = 5.02$ TeV and in Xe + Xe collisions at $\sqrt{s} = 5.44$ TeV. Calculations are performed for versions with and without nucleon meson cloud. The fraction of the binary collisions, α, has been fitted to the data on $dN_{ch}/d\eta$ in Pb + Pb collisions. We obtain $\alpha \approx 0.09(0.13)$ with (without) meson cloud. The effect of meson cloud on the $dN_{ch}/d\eta$ is relatively small. For Xe + Xe collisions for 0–5% centrality bin we obtain $dN_{ch}/d\eta \approx 1149$ and 1134 with and without meson cloud, respectively. We obtain $\varepsilon_2(\text{Xe})/\varepsilon_2(\text{Pb}) \sim 1.45$ for most central collisions, and $\varepsilon_2(\text{Xe})/\varepsilon_2(\text{Pb})$ close to unity at $c \gtrsim 20\%$. We find a noticeable increase of the eccentricity in Xe + Xe collisions at small centralities due to the prolate shape of the Xe nucleus. The triangularity in Xe + Xe collisions is bigger than in Pb + Pb collisions at $c \lesssim 70\%$. We obtain $\varepsilon_3(\text{Xe})/\varepsilon_3(\text{Pb}) \sim 1.3$ at $c \lesssim 1\%$.

1 Introduction

It is believed that production of soft particles in AA collisions at RHIC and LHC energies occurs via formation of the quark-gluon plasma (QGP) that expands hydrodynamically as a near-ideal liquid [1,2]. Hydrodynamic models have been successfully used for description of the data from RHIC and LHC on centrality dependence of hadron multiplicities and flow effects in AA collisions. The currently available LHC data on AA collisions have been obtained for Pb + Pb collisions at $\sqrt{s} = 2.76$ and 5.02 TeV. Recently at the LHC there has been performed a run for Xe + Xe collisions ($A = 129$) at $\sqrt{s} = 5.44$ TeV. The data from this run will allow to study variation of the A-dependence of soft hadron production in AA collisions. One can expect that the flow effects for Xe + Xe collisions should be stronger than for Pb + Pb collisions because fluctuations in the initial entropy density should increase for nuclei with a smaller nucleon number. For this reason the data on Xe + Xe collisions are of great interest for testing the hydrodynamic picture of the QGP fireball evolution. The Xe + Xe collisions at $\sqrt{s} = 5.44$ TeV have been discussed recently in Refs. [3,4].

The hydrodynamic simulations of AA collisions require imposing the initial conditions for the entropy/energy distribution at the QGP production time $\tau_0 \sim 0.5-1$ fm [5,6]. One of the popular approach for setting the initial conditions for the QGP fireball in AA collisions is the Monte-Carlo Glauber (MCG) wounded nucleon model [7–10]. In Refs. [11,12] we have developed a version of the MCG wounded nucleon model for nucleons with meson cloud. The meson-baryon Fock components of the nucleon play an important role in the flavor dependence of nucleon parton distribution functions (PDFs) in deep inelastic scattering [13], and allow to explain the violation of the Gottfried sum rule [13]. It is important that, similarly to the wounded nucleon model with constituent quarks [14–19], the meson degrees of freedom lead to a nonlinear increase of $dN_{ch}(AA)/d\eta$ with the number of the wounded nucleons [12]. This effect should emerge independently of the specific mechanism of inelastic interactions. It is important that, contrary to the MCG models with the quark subnucleon degrees of freedom, the interaction of the meson components is better understood, say, within the quark-gluon string model [20,21]. Similarly to the ordinary two-component MCG model without meson cloud [9] the model [11,12] accounts for the contributions from soft interaction (participant wounded nucleons) and from hard binary collisions [22]. However, the results of Refs. [11,12] show that in the presence of the meson-baryon Fock components the required fraction of the binary collisions, α, becomes smaller. The results of Ref. [12] show that the meson cloud may improve somewhat agreement with the data on the dependence of the elliptic flow on the charged multiplicity for very small centralities defined via the ZDCs signals for col-

[a] e-mail: bgz@itp.ac.ru

lisions of the deformed uranium nuclei at $\sqrt{s} = 0.193$ TeV [23]. In the present paper we apply the model of Refs. [11,12] to obtain predictions for Xe + Xe collisions at $\sqrt{s} = 5.44$ TeV. To fix the parameters of the model we use the data on pp and Pb + Pb collisions.

The plan of the paper is as follows. In Sect. 2 we outline the theoretical framework. In Sect. 3 we present the numerical results. We give conclusions in Sect. 4.

2 Outline of the model

In this section we briefly sketch our MCG scheme. We refer the reader to Ref. [12] for more details.

We represent the physical nucleon wave function $|N_{phys}\rangle$ in the infinite-momentum frame (IFM) as the Fock-state composition of a bare nucleon $|N\rangle$ and an effective two-body meson-baryon $|MB\rangle$ state

$$|N_{phys}\rangle = \sqrt{1 - n_{MB}}|N\rangle + \int dx d\mathbf{k} \Psi_{MB}(x, \mathbf{k})|MB\rangle\,, \quad (1)$$

where x is the fractional longitudinal meson momentum in the physical nucleon, $\mathbf{k}$ is the transverse meson momentum, Ψ_{MB} is the IMF (light-cone) wave function of the MB Fock state, and

$$n_{MB} = \int dx d\mathbf{k} |\Psi_{MB}(x, \mathbf{k})|^2 \quad (2)$$

is the total weight of the MB Fock state. The previous analyses of the meson cloud effects in deep inelastic scattering (for a review, see Ref. [13]) show that the total weight of the meson-baryon Fock states in the nucleon is $\sim 40\%$. Due to this, we take for the probability of the effective MB state $n_{MB} = 0.4$. Since the meson-baryon component is dominated by the pion-nucleon πN state [13], we calculate the IMF distribution of the effective MB state for the γ_5 spin vertex. As in the analyses of the deep inelastic scattering [13], we introduce a phenomenological vertex formfactor, F, to account for the internal structure of the hadrons. We take it in the form [13]

$$F = \left(\frac{\Lambda^2 + m_N^2}{\Lambda^2 + M_{\pi N}^2}\right)^2\,, \quad (3)$$

where $M_{\pi N}$ is the invariant mass of the πN system. We take $\Lambda = 1.3$ GeV, supported by the analysis [24] of the data on the process $pp \to nX$. This value, at the same time, is also supported by the data on the violation of the Gottfried sum rule for the nucleon PDFs [13]. Note, however, that our results are not very sensitive to the value of Λ.

In our model, as in the well known version of the MCG wounded nucleon model at the elementary nucleon-level GLISSANDO [9], the entropy is deposited in the soft sources from participants (related to soft interactions) and in the hard sources from the binary collisions, related to hard reactions, between the colliding particles. However, in our scheme the inelastic interaction of the physical nucleons from the colliding objects may occur as $N + N$, $N + MB$, $MB + N$ and $MB + MB$ collisions. Because at high energy the midrapidity multiplicity density for all baryons and mesons should be similar, we assume that the constituents M and B in the MB effective Fock state interact like a pion and a nucleon, respectively. We assume that the inelastic cross sections for the bare baryon and meson states obey the constituent quark counting rule $4\sigma_{in}^{NN} = 6\sigma_{in}^{MB} = 9\sigma_{in}^{MM}$. We use the Gaussian impact parameter profile for the probability of ab inelastic interaction of the bare constituents

$$P_{ab}(\rho) = \exp\left(-\pi\rho^2/\sigma_{in}^{ab}\right)\,. \quad (4)$$

The parameter σ_{in}^{NN} has been adjusted to fit the experimental inelastic pp cross section for non-single-diffractive (NSD) events. The use of the data on the NSD pp events is reasonable because the diffractive events do not contribute to the multiplicity in the midrapidity region that we consider.

We assume isentropic evolution of the QGP fireball. Then the initial entropy rapidity density produced in an AA collision is proportional to the final charged multiplicity pseudorapidity density

$$dS/dy = C dN_{ch}/d\eta\,, \quad (5)$$

where $C \approx 7.67$ [25]. For this reason in our calculations we consider the soft and the hard sources of the entropy as direct sources of the multiplicity density. We will consider the charged multiplicity density $dN_{ch}/d\eta$ at the central pseudorapidity $\eta = 0$ defined as N_{ch} in the unit pseudorapidity window $|\eta| < 0.5$. We assume that the sources generated in all possible collisions of the bare constituents (i.e., for NN, MN, and MM collisions) have the same intensity. This approximation is supported by the calculations within the quark-gluon string model [20,21] which show that the difference between the midrapidity multiplicity density generated in NN, MN and MM interactions is small.

We model the fluctuations of the charged particle density generated by the sources by the Gamma distribution

$$\Gamma(n, \langle n\rangle) = \left(\frac{n}{\langle n\rangle}\right)^{\kappa-1} \frac{\kappa^\kappa \exp\left[-n\kappa/\langle n\rangle\right]}{\langle n\rangle \Gamma(\kappa)}\,, \quad (6)$$

which is widely used in the MCG simulations. For each soft source corresponding to a wounded constituent the contribution to the multiplicity density is given by $(1 - \alpha)\Gamma/2$, and for a hard source from a binary collision it is simply Γ. However, for each pair of wounded particles the probability

of a hard binary collision is suppressed by α. The parameters $\langle n\rangle$ and κ have been adjusted to reproduce the experimental pp data on the mean charged multiplicity and its variance in the unit pseudorapidity window $|\eta| < 0.5$, and the value of α has been fitted from the data on Pb + Pb collisions (see below).

For calculations of the multiplicity density $dN_{ch}/d\eta$ one can use the approximation of the point-like sources. But the smearing of the sources may be important in calculations of the initial anisotropy coefficients ε_n of the QGP fireball, which in terms of the spacial entropy distribution $\rho_s = dS/dyd\boldsymbol{\rho}$ read [26,27]

$$\varepsilon_n = \frac{\left|\int d\boldsymbol{\rho}\rho^n e^{in\phi}\rho_s(\boldsymbol{\rho})\right|}{\int d\boldsymbol{\rho}\rho^n\rho_s(\boldsymbol{\rho})}\,, \tag{7}$$

where the transverse vectors $\boldsymbol{\rho}$ are calculated in the c.m. frame, i.e., $\int d\boldsymbol{\rho}\boldsymbol{\rho}\rho_s(\boldsymbol{\rho}) = 0$. To model the smearing of the sources we use a Gaussian source distribution

$$\exp\left(-\boldsymbol{\rho}^2/\sigma^2\right)/\pi\sigma^2\,. \tag{8}$$

We perform calculations for $\sigma = 0.7$ and 0.4 fm. The results for the anisotropy coefficients become sensitive to σ only for very peripheral AA collisions.

We perform calculations for the Woods–Saxon nuclear distributions with the hard-core repulsion. Following to Ref. [9], we take for the hard-core radius $d = 0.9$ fm. For the one-body Woods–Saxon distributions for ^{129}Xe we use the θ-dependent nuclear density

$$\rho_A(r,\theta) = \frac{\rho_0}{1+\exp[(r-R_A(\theta)/a]}\,, \tag{9}$$

$$R_A(\theta) = R[1+\beta_2 Y_{20}(\theta)+\beta_4 Y_{40}(\theta)] \tag{10}$$

with Y_{20} and Y_{40} the spherical harmonics, with $\beta_2 = 0.162$, and $\beta_4 = -0.003$ [28]. For the ^{208}Pb nucleus we use the ordinary spherically symmetric Woods–Saxon formula with a θ-independent ($\beta_{02} = \beta_{04} = 0$) radius R_A. For the nucleus radii we use the formula $R = (1.1A^{1/3} - 0.656/A^{1/3})$ fm, and take $a = 0.459$ fm borrowed from Ref. [9]. To understand the role of the prolate shape of the Xe nucleus, we also perform calculations for Xe + Xe collisions using the spherically symmetric Woods–Saxon formula. As will be seen from our results the prolate shape of the Xe nucleus increases noticeably the ellipticity ε_2 at small centralities.

3 Results

The direct pp data on the charged multiplicity and inelastic cross section at $\sqrt{s} = 5.02$ and 5.44 TeV are absent. We obtained $dN_{ch}/d\eta$ for these energies with the help of the power law interpolation $dN_{ch}/d\eta \propto s^{\delta}$ between the ALICE data [29] at $\sqrt{s} = 2.76$ TeV ($dN_{ch}/d\eta \approx 4.63$) and at $\sqrt{s} = 7$ TeV ($dN_{ch}/d\eta = \approx 5.74$) for the charged multiplicity in NSD events. It gives $dN_{ch}/d\eta[\sqrt{s} = 5.02\,, 5.44\,\text{TeV}] \approx [5.32,\ 5.42]$. We used a similar procedure to obtain the NSD pp inelastic cross sections at $\sqrt{s} = 5.02$ and 5.44 TeV from the ALICE [30] results for $\sqrt{s} = 2.76$ TeV ($\sigma_{in}^{NSD} \approx 50.24$ mb) and 7 TeV ($\sigma_{in}^{NSD} \approx 58.56$ mb). We obtained the values: $\sigma_{in}^{pp}[\sqrt{s} = 5.02\,, 5.44\,\text{TeV}] \approx [54.44,\ 56.18]$ mb.

Since the difference in the energy between Xe + Xe collisions at $\sqrt{s} = 5.44$ TeV and Pb + Pb collisions at $\sqrt{s} = 5.02$ TeV is relatively small, we use the same fraction of the binary collisions α for $\sqrt{s} = 5.02$ and 5.44 TeV. We determine α from fits to the ALICE [31] data on the centrality dependence of the midrapidity charged multiplicity density N_{ch} at $|\eta| < 0.5$ in Pb + Pb collisions $\sqrt{s} = 5.02$ TeV. As in Ref. [12], we use a two step procedure. First, we fitted $\langle n\rangle$ and κ for a broad set of α to the N_{ch} in pp collisions imposing the condition $N_{ch}/D = 1$, which is well satisfied for $|\eta| < 0.5$ window [29,32]. Then, we used the values of $\langle n\rangle$ and κ to fit the parameter α from the Pb + Pb data. This procedure gives $\alpha \approx 0.09$ and $\alpha \approx 0.13$ for the scenarios with and without meson cloud, respectively. The parameters of the Gamma distribution (6) obtained from the fit with meson cloud to the pp data for the above optimal value $\alpha = 0.09$ read: $\langle n\rangle \approx 4.69(4.8)$, $\kappa \approx 0.516(0.524)$ for $\sqrt{s} = 5.02(5.44)$ TeV. For the scenario without meson cloud for the optimal value $\alpha = 0.13$ we obtained $\kappa \approx 0.56(0.56)$ for $\sqrt{s} = 5.02(5.44)$ TeV, (in the version without meson cloud the value of $\langle n\rangle$ is simply equal to the experimental N_{ch} for pp collisions).

In Fig. 1 we show the results of our fit to the ALICE data on the centrality dependence of the midrapidity charged multiplicity density in Pb + Pb collisions at $\sqrt{s} = 5.02$ TeV [31] obtained by Monte Carlo generation of $\sim 2\cdot 10^6$ events for the scenarios with and without meson cloud. The scenario with meson cloud gives somewhat better agreement with the data (χ^2/d.p ≈ 0.1) as compared to the version without meson cloud (χ^2/d.p ≈ 0.3).

In Fig. 2 we show our predictions for centrality dependence of the charged multiplicity in Xe + Xe collisions at $\sqrt{s} = 5.44$ TeV obtained with and without meson cloud. The difference between two version is relatively small. For intermediate centrality region the meson cloud increases $dN_{ch}/d\eta$ by $\sim 5\%$. For the 0–5% centrality $dN_{ch}/d\eta \approx 1149$ and 1134 for the versions with and without meson cloud, respectively. It is smaller by $\sim 6-7\%$ than the charged multiplicity density obtained in Ref. [4]. From Figs. 1 to 2 one sees that as compared to Pb + Pb collisions at $\sqrt{s} = 5.02$ TeV for Xe + Xe 0-5% central collisions at $\sqrt{s} = 5.44$ TeV, $dN_{ch}/d\eta$ becomes smaller by a factor of ~ 1.7. That corresponds to decrease of the initial QGP temperature by a factor of ~ 1.2. A remark is in order here. The curves in Fig. 2 are obtained under assumption of an isentropic flow. But we

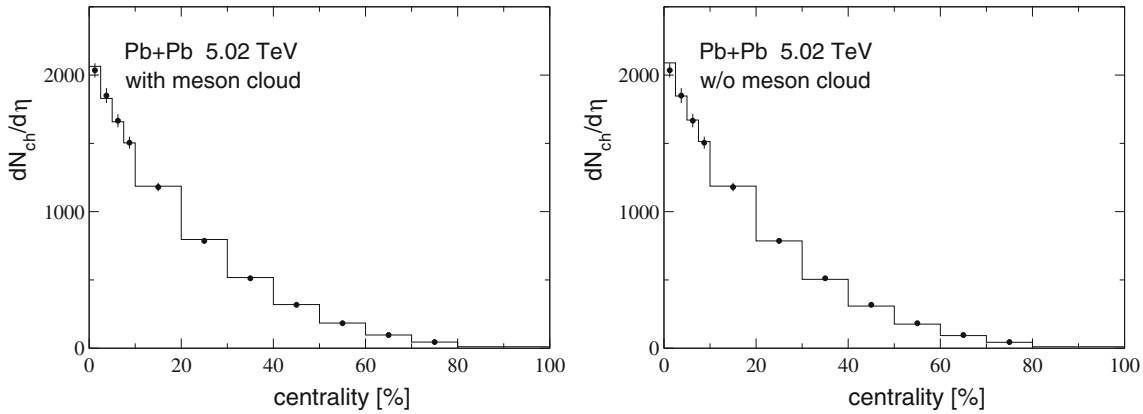

Fig. 1 Centrality dependence of midrapidity $dN_{ch}/d\eta$ for Pb + Pb collisions at $\sqrt{s} = 5.02$ TeV. Left: MCG simulation for the scenario with meson cloud at $\alpha = 0.09$. Right: MCG simulation for the scenario without meson cloud at $\alpha = 0.13$. Data are from ALICE [31]

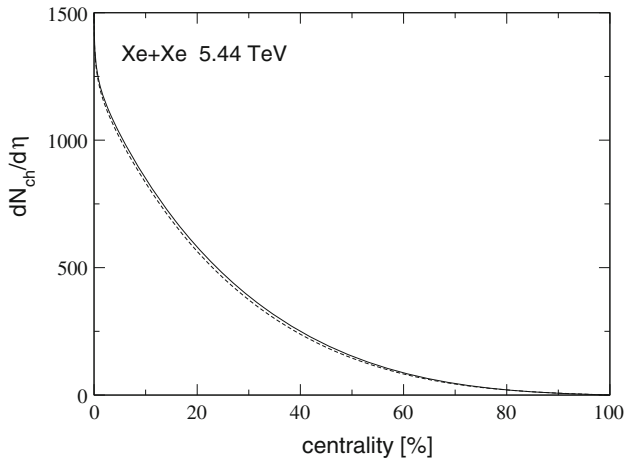

Fig. 2 Centrality dependence of midrapidity $dN_{ch}/d\eta$ for Xe + Xe collisions at $\sqrt{s} = 5.44$ TeV obtained for the scenarios with (solid) meson cloud at $\alpha = 0.09$ and without (dashed) meson cloud at $\alpha = 0.13$

fitted the parameters of the model from the data on Pb + Pb collisions also ignoring the non-isentropic effects. Since these effects are weak, possible errors in the extrapolation of the results from Pb + Pb to Xe + Xe collisions should be small.

In Figs. 3 and 4 we present the results for the rms ε_2 (the rms ε_n is often denoted $\varepsilon_n\{2\}$, for clarity, we omit $\{2\}$) versus centrality for Pb + Pb at $\sqrt{s} = 5.02$ TeV and Xe + Xe at $\sqrt{s} = 5.44$ TeV for two version of the model. The anisotropy coefficients depend on the smearing parameter σ in (8). We present the results for two values of the Gaussian width of the sources $\sigma = 0.7$ and 0.4 fm. From Figs. 3 to 4 one sees that for small centralities the results with and without meson cloud are close to each other. For intermediate centralities the version with meson cloud gives a little smaller ε_2. For very peripheral collisions with centrality $\gtrsim 80\%$ the model without meson cloud gives bigger ε_2. From comparing the results in Figs. 3 and 4 one can

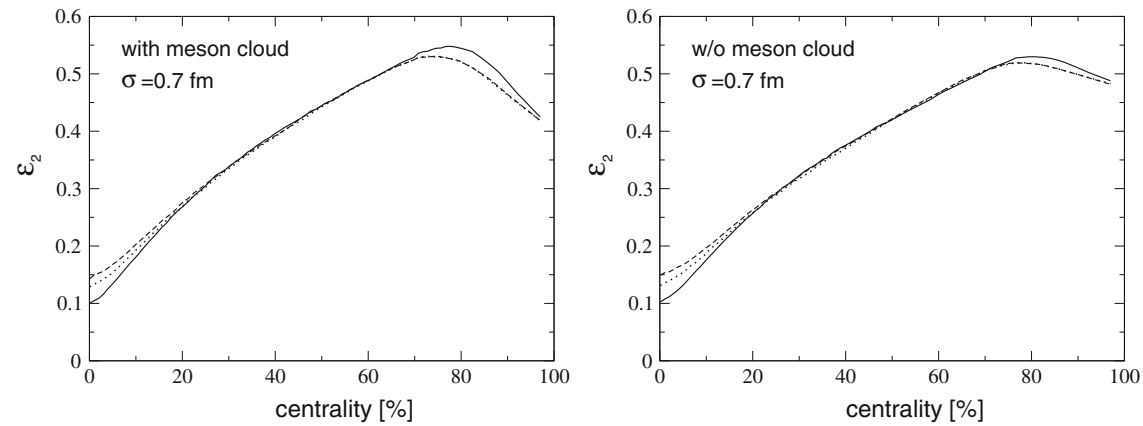

Fig. 3 Centrality dependence of the rms ε_2 for the Gaussian source distribution (8) for $\sigma = 0.7$ fm for Pb + Pb collisions at $\sqrt{s} = 5.02$ TeV (solid) and Xe + Xe collisions at $\sqrt{s} = 5.44$ TeV for the θ-dependent (dashed) and symmetric Woods–Saxon distribution (dotted). Left: the version with meson cloud at $\alpha = 0.09$. Right: the version without meson cloud at $\alpha = 0.13$

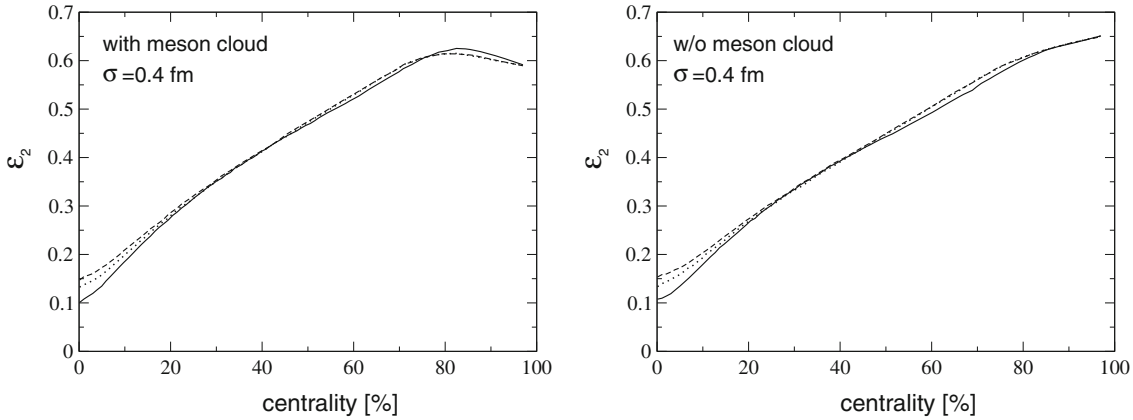

Fig. 4 Same as in Fig. 3 but for $\sigma = 0.4$ fm

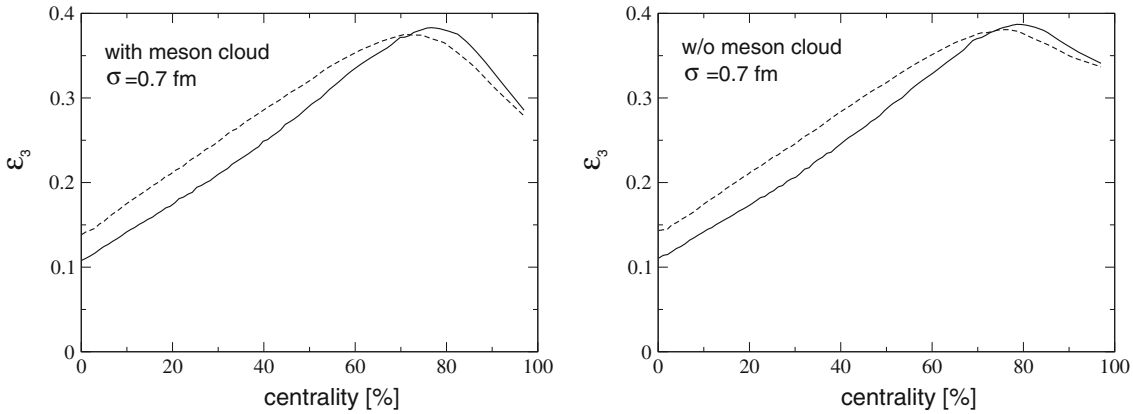

Fig. 5 Centrality dependence of the rms ε_3 for the Gaussian source distribution (8) for $\sigma = 0.7$ fm for Pb + Pb collisions at $\sqrt{s} = 5.02$ TeV (solid) and Xe + Xe collisions at $\sqrt{s} = 5.44$ TeV for the θ-dependent Woods–Saxon distribution (dashed). Left: the version with meson cloud at $\alpha = 0.09$. Right: the version without meson cloud at $\alpha = 0.13$

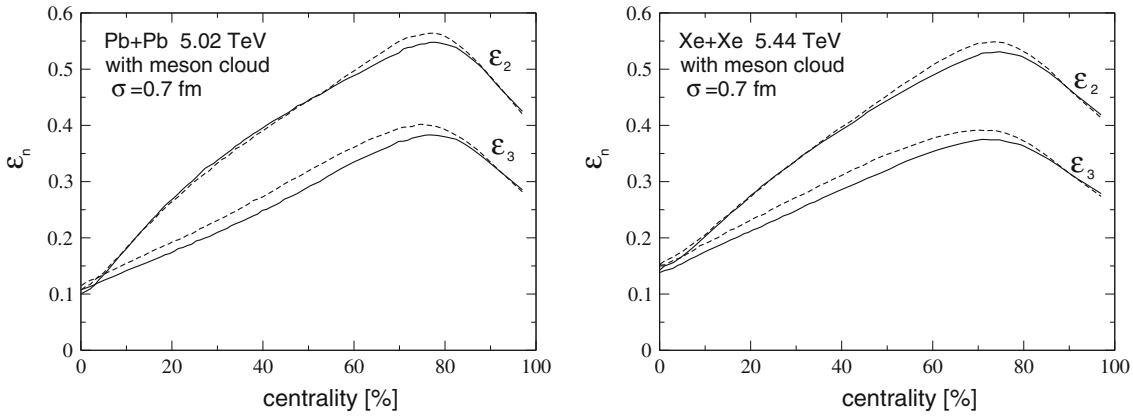

Fig. 6 Centrality dependence of the rms $\varepsilon_{2,3}$ for the version with meson cloud with the Gaussian source distribution (8) for $\sigma = 0.7$ fm in Pb + Pb collisions at $\sqrt{s} = 5.02$ TeV (left) and in Xe + Xe collisions at $\sqrt{s} = 5.44$ TeV (right) for the θ-dependent Woods–Saxon distribution with (solid) and without (dashed) the hard-core repulsion

see that the value of the smearing width becomes important at $c \gtrsim 30 - 40\%$, where the eccentricity grows with decreasing σ. From Figs. 3 to 4 one sees that for the most central collisions $c \lesssim 5\%$ $\varepsilon_s(\mathrm{Xe})/\varepsilon_2(\mathrm{Pb}) \sim 1.3 - 1.4$, and $\varepsilon_s(\mathrm{Xe})/\varepsilon_2(\mathrm{Pb})$ becomes close to unity at $c \gtrsim 30\%$. For very peripheral collisions with $c \gtrsim 75\%$ $\varepsilon_2(\mathrm{Xe})$ becomes a little

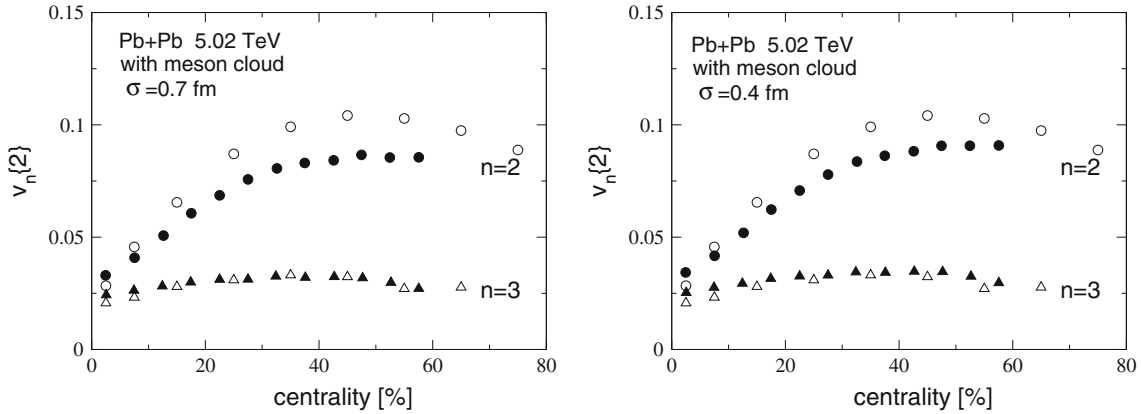

Fig. 7 Centrality dependence of $v_2\{2\}$ (filled circles) and $v_3\{2\}$ (filled triangles) for Pb + Pb collisions at $\sqrt{s} = 5.02$ TeV obtained from $\varepsilon_{2,3}$ with meson cloud for $\sigma = 0.7$ (left) and 0.4 fm (right) with the help of the linear response approximation (see text for explanations) using the results of the hydrodynamic simulations of Ref. [3]. Open circles and triangles are $v_{2,3}\{2\}$ from ALICE [41]

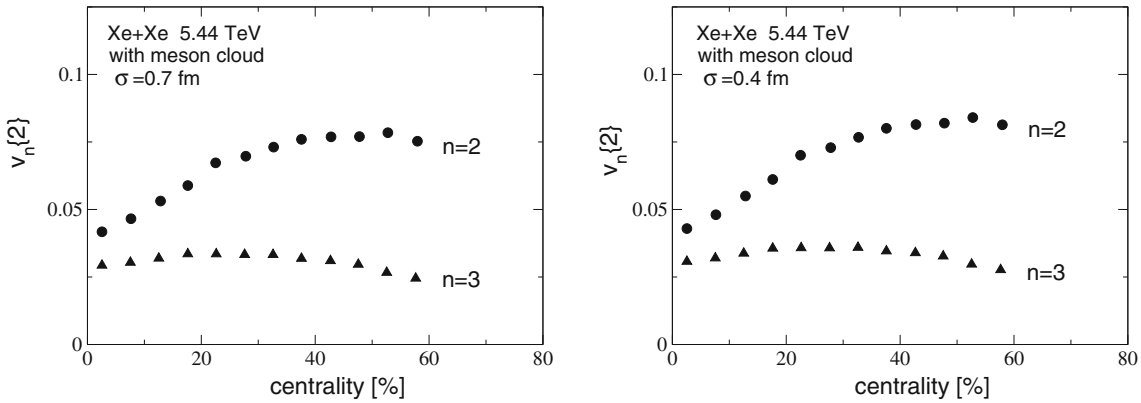

Fig. 8 Same as in Fig. 7 but for Xe + Xe collisions at $\sqrt{s} = 5.44$ TeV

smaller than ε_2(Pb). From Figs. 3 to 4, by comparing the curves for Xe + Xe collisions obtained for the asymmetric and symmetric Woods–Saxon distribution, one can see that the effect of the prolate shape of the Xe nucleus on the eccentricity becomes important at $c \lesssim 20\%$. For most central collisions the asymmetric Woods–Saxon distribution increases the eccentricity by $\sim 12\%$. This is due to the highly overlapping body-body collisions of the nucleus ellipsoids, that lead naturally to an asymmetric entropy deposition.

In Fig. 5 we present the results for the rms triangularity ε_3 for $\sigma = 0.7$ fm. One can see that both for Pb + Pb and Xe + Xe collisions the triangularity for the versions with and without meson cloud are very similar for small and intermediate centralities. For very peripheral collisions $c \gtrsim 80\%$ ε_3 for the version without meson cloud becomes bigger. Our calculations show that for Xe + Xe collisions the effect of the prolate form of the Xe nucleus is very small. For this reason we do not plot in Fig. 5 the results for Xe + Xe collisions for the symmetric Woods–Saxon distribution. From Fig. 5 one sees that ε_3(Xe)/ε_3(Pb) ~ 1.3 for most central collisions, and decreases to unity at $c \sim 70\%$.

The results shown in Figs. 1, 2, 3, 4 and 5 have been obtained for the Monte-Carlo sampling with the nuclear distribution with the hard-core radius $d = 0.9$ fm. It is evident that the presence of the hard-core repulsion should reduce the fluctuations of the nuclear matter density in the colliding nuclei, that can suppress the effect of the fluctuations in the initial entropy deposition. To study the role of the hard-core repulsion we also performed the calculations for $d = 0$. In this case we also use the parameters of the Woods–Saxon distribution from the analysis [9]: $R = (1.12A^{1/3} - 0.86/A^{1/3})$ fm, and $a = 0.54$ fm. Calculations in this version show that the effect of the hard-core repulsion on the centrality dependence of the charged multiplicity density is small. But the effect is stronger for the anisotropy coefficients. It is illustrated in Fig. 6 where we plot $\varepsilon_{2,3}$ versus centrality obtained with (solid) and without (dashed) the hard-core repulsion for the version with meson cloud at $\sigma = 0.7$ fm. From Fig. 6 one sees that the effect of the hard-core is bigger for the purely fluctuation-driven quantity ε_3. At $c \lesssim 70\%$ the hard-core reduces ε_3 by $\sim 10\%$ both for Pb + Pb and Xe + Xe collisions. For the eccentricity ε_2 the effect of the hard-core is

noticeable for small centralities. In this region ε_2 is also dominated by fluctuations, and the hard-core repulsion reduces ε_2 by $\sim 10\%$ both for Pb + Pb and Xe + Xe collisions.

Our results for the initial $\varepsilon_{2,3}$ for Pb + Pb and Xe + Xe collisions do not differ strongly from that of Refs. [3,4]. The analysis [3] is based on the TRENTO Monte-Carlo model [33,34], and [4] is based on the so called EKRT [35] model with mini-jet parton production. For intermediate centralities $c \sim 50\%$ our ε_2 for $\sigma = 0.7$ fm is smaller than that of Refs. [3,4] by $\sim 10-15\%$. But for small centralities our predictions for $\varepsilon_{2,3}$ are somewhat bigger. Note that in Refs. [3,4] the calculations for Xe + Xe collisions have been performed only with the symmetric Woods–Saxon nuclear distribution. For this reason the grows of the ratio $\varepsilon_2(\text{Xe})/\varepsilon_2(\text{Pb})$ at $c \to 0$ in Refs. [3,4] is not so strong as in our results.

The event by event hydrodynamic modeling of AA collisions shows that, except for very peripheral collisions, to a good approximation $v_n \approx k_n \varepsilon_n$ for $n = 2,\ 3$ [36–39] (for a comprehensive review, see, e.g., Ref. [40]). This linear response approximation works better for v_2 [38,39]. In the present paper we do not perform the hydrodynamic simulation of Pb + Pb and Xe + Xe collisions that are necessary for accurate calculations of v_n. To obtain predictions for the flow coefficients via our MCG results for ε_n we use the above linear response relation with $k_{2,3}$ defined via the ratio of $v_{2,3}\{2\}$ to rms $\varepsilon_{2,3}$ obtained for Pb + Pb collisions at $\sqrt{s} = 5.02$ TeV and for Xe + Xe collisions at $\sqrt{s} = 5.44$ TeV in the hydrodynamic calculations with the shear viscosity over entropy ratio $\eta/s = 0.047$ in Ref. [3].[1] In Fig. 7 we compare $v_{2,3}\{2\}$ obtained in this way for Pb + Pb collisions at $\sqrt{s} = 5.02$ TeV with the results from ALICE [41]. We used our anisotropy coefficients $\varepsilon_{2,3}$ obtained with meson cloud for the Woods–Saxon distribution with the hard-core repulsion for the smearing width $\sigma = 0.7$ and 0.4 fm. From Fig. 7 one sees that for $n = 2$ the theoretical results underestimate the data by $\sim 10-20\%$ at $c \sim 30-60\%$, but for $n = 3$ the agreement is quite reasonable. The theoretical predictions for $v_{2,3}\{2\}$ in Xe + Xe collisions at $\sqrt{s} = 5.44$ TeV are shown in Fig. 8. The relation between our predictions for $v_n\{2\}$ to that of Ref. [3] similar to the situation with predictions for ε_n. For most central collisions, due to bigger values of $\varepsilon_{2,3}$, we predict somewhat bigger $v_{2,3}\{2\}$ (by $\sim 5\%$ for $\sigma = 0.7$ fm and by $\sim 10\%$ for $\sigma = 0.4$ fm).

The predictions in Figs. 7 and 8 correspond to the version with the hard-core repulsions. From the curves in Fig. 6 one sees that the hard-core repulsion reduces the initial anisotropy coefficients due some reduction of the the nuclear density fluctuations. However, one should bear in mind that the dynamical effects, which can affect the long range fluctuations of the nuclear density, are completely ignored in our Monte-Carlo scheme. For this reason the predictions for the initial anisotropy coefficients may be questioned (especially for the fluctuation driven quantity ε_3). Indeed, it is well known [42,43] that the dynamical long range fluctuations of the nuclear matter in heavy nuclei are dominated by the giant resonances, e.g., by the giant dipole, monopole, and quadrupole resonances. In Ref. [44] we have demonstrated that for the dipole mode of the ^{208}Pb nucleus the classical treatment based on the Monte-Carlo simulation with the Woods–Saxon nuclear density overestimates the fluctuations of the dipole moment squared by a factor of ~ 5. The situation with the dynamical quantum effects for the monopole and quadrupole collective modes, that potentially may also be important, remains unclear. It would be of great interest to study the role of the dynamical quantum effects due to the giant resonances on the fluctuations of the entropy deposition in AA collisions (of course, these effects may also be important for calculations in other approaches, say, in the EKRT model [35], TRENTO model [34], or in the color glass condensate scheme [45,46]). We leave this for future work.

4 Conclusions

We have studied the centrality dependence of the charged midrapidity multiplicity density in Pb + Pb collisions at $\sqrt{s} = 5.02$ TeV and in Xe + Xe collisions at $\sqrt{s} = 5.44$ TeV within the MCG model with and without meson cloud developed in Ref. [12]. The parameters of the model have been fixed to the ALICE data [31] on $dN_{ch}/d\eta$ in Pb + Pb collisions. We obtained the fraction of the binary collisions $\alpha \approx 0.09(0.13)$ with (without) meson cloud. With these parameters we give predictions for future LHC data on Xe + Xe collisions at $\sqrt{s} = 5.44$ TeV. We find that the effect of the meson cloud on the $dN_{ch}/d\eta$ is relatively small. For Xe + Xe collisions the meson cloud increases $dN_{ch}/d\eta$ by $\sim 5\%$ in the intermediate centrality region. For the 0-5% centrality bin we obtained $dN_{ch}/d\eta \approx 1149$ and 1134 with and without meson cloud, respectively. As compared to Pb + Pb collisions at $\sqrt{s} = 5.02$ TeV for Xe + Xe 0–5% central collisions at $\sqrt{s} = 5.44$ $dN_{ch}/d\eta$ becomes smaller by a factor of ~ 1.7. It corresponds to decrease of the initial QGP temperature by a factor of ~ 1.2.

Both for Pb + Pb and Xe + Xe collisions we do not find a significant effect of the meson cloud on the $\varepsilon_{2,3}$ at $c \lesssim 70\%$. But the meson cloud reduces $\varepsilon_{2,3}$ for very peripheral collisions. We find that the ratio of the eccentricity in Xe + Xe collisions to that for Pb + Pb collisions is close to unity at $c \gtrsim 20\%$, but it becomes bigger than unity at $c \lesssim 20\%$. We obtained $\varepsilon_2(\text{Xe})/\varepsilon_2(\text{Pb}) \sim 1.45$ for most central collisions ($c \lesssim 1\%$). We predict a noticeable increase of the eccentricity

[1] In principle, it is clear that this procedure should be quite accurate even beyond the linear response picture (say, when the cubic terms become important [39]) because the difference between our predictions for $\varepsilon_{2,3}$ and that of Ref. [3] is not very large.

in Xe + Xe collisions at small centralities due to the prolate shape of the Xe nucleus. This effect gives $\sim$ 50% to the difference between the eccentricity in most central Xe + Xe and Pb + Pb collisions.

We find that at $c \lesssim 70\%$ the triangularity in Xe + Xe collisions is bigger than in Pb + Pb collisions. We obtain $\varepsilon_3(\mathrm{Xe})/\varepsilon_3(\mathrm{Pb}) \sim 1.3$ at $c \lesssim 1\%$ and $\varepsilon_3(\mathrm{Xe})/\varepsilon_3(\mathrm{Pb}) \sim 1.1$ at $c \sim 50\%$. We have investigated the effect of the hard-core repulsion in the Monte-Carlo sampling of the nuclear distributions. We found that the hard-core repulsion gives a relatively small effect on the charged multiplicity density. But its effect is sizeable for the anisotropy coefficients $\varepsilon_{2,3}$. For ε_2 the effect of the hard-core is noticeable for small centralities where ε_2 is dominated by fluctuations. For most central collisions the hard-core repulsion reduces ε_2 by $\sim 10\%$ both for Pb + Pb and Xe + Xe collisions. The triangularity ε_3 is reduced by the hard-core repulsion by $\sim 10\%$ at $c \lesssim 70\%$ both for for Pb + Pb and Xe + Xe collisions.

To obtain predictions for the flow coefficients via our MCG results for ε_n we have used the linear response relation $v_n \approx k_n \varepsilon_n$ with k_n defined via the ratio of $v_{2,3}\{2\}$ to rms $\varepsilon_{2,3}$ obtained in the recent hydrodynamic analysis [3]. The results for $v_{2,3}\{2\}$ obtained in this way for Pb + Pb collisions at $\sqrt{s} = 5.02$ TeV are in reasonable agreement with the data from ALICE [41].

Funded by SCOAP[3].

References

1. P. Huovinen, Int. J. Mod. Phys. E **22**, 1330029 (2013). arXiv:1311.1849 **(and references therein)**
2. R. Derradi de Souza, T. Koide, T. Kodama, Prog. Part. Nucl. Phys. **86**, 35 (2016). arXiv:1506.03863 **(and references therein)**
3. G. Giacalone, J. Noronha-Hostler, M. Luzum, U. Sao Paulo, J.Y. Ollitrault, Phys. Rev. C **97**, 034904 (2018). arXiv:1711.08499
4. K.J. Eskola, H. Niemi, R. Paatelainen, K. Tuominen, Phys. Rev. C **97**, 034911 (2018). arXiv:1711.09803
5. U. Heinz, R. Snellings, Ann. Rev. Nucl. Part. Sci. **63**, 123 (2013). arXiv:1301.2826
6. H. Song, S.A. Bass, U. Heinz, T. Hirano, Phys. Rev. C **83**, 054910 (2011). arXiv:1101.4638 **(Erratum. Phys. Rev. C 86, 059903 (2012))**
7. B. Alver, M. Baker, C. Loizides, P. Steinberg. arXiv:0805.4411
8. W. Broniowski, M. Rybczynski, P. Bozek, Comput. Phys. Commun. **180**, 69 (2009). arXiv:0710.5731
9. M. Rybczynski, G. Stefanek, W. Broniowski, P. Bozek, Comput. Phys. Commun. **185**, 1759 (2014). arXiv:1310.5475
10. C. Loizides, J. Kamin, D. d'Enterria, Phys. Rev. C **97**, 054910 (2018). arXiv:1710.07098
11. B.G. Zakharov, JETP Lett. **104**, 6 (2016). arXiv:1605.06012
12. B.G. Zakharov, J. Exp. Theor. Phys. **124**, 860 (2017). arXiv:1611.05825
13. J. Speth, A.W. Thomas, Adv. Nucl. Phys. **24**, 83 (1997)
14. A. Bialas, W. Czyz, W. Furmanski, Acta Phys. Pol. B **8**, 585 (1977)
15. A. Bialas, W. Czyz, Acta Phys. Pol. B **10**, 831 (1979)
16. S. Eremin, S. Voloshin, Phys. Rev. C **67**, 064905 (2003). arxiv:nucl-th/0302071
17. P. Bozek, W. Broniowski, M. Rybczynski, Phys. Rev. C **94**, 014902 (2016). arXiv:1604.07697
18. A. Bialas, A. Bzdak, Phys. Rev. C **77**, 034908 (2008). arXiv:0707.3720
19. C. Loizides, Phys. Rev. C **94**, 024914 (2016). arXiv:1603.07375
20. A.B. Kaidalov, M.G. Poghosyan, Eur. Phys. J. C **67**, 397 (2010). arXiv:0910.2050
21. A. Capella, E.G. Ferreiro, Eur. Phys. J. C **72**, 1936 (2012). arXiv:1110.6839
22. D. Kharzeev, M. Nardi, Phys. Lett. B **507**, 121 (2001). arxiv:nucl-th/0012025
23. L. Adamczyk et al., STAR Collaboration, Phys. Rev. Lett. **115**, 222301 (2015). arXiv:1505.07812
24. H. Holtmann, A. Szczurek, J. Speth, Nucl. Phys. A **596**, 631 (1996). arxiv:hep-ph/9601388
25. B. Müller, K. Rajagopal, Eur. Phys. J. C **43**, 15 (2005). arxiv:hep-ph/0502174
26. D. Teaney, L. Yan, Phys. Rev. C **83**, 064904 (2011). arXiv:1010.1876
27. E. Retinskaya, M. Luzum, J.-Y. Ollitrault, Nucl. Phys. A **926**, 152 (2014). arXiv:1401.3241
28. P. Möller, A.J. Sierk, T. Ichikawa, H. Sagawa, Atom. Data Nucl. Data Tables **109–110**, 1 (2016). arXiv:1508.06294
29. J. Adam, et al., ALICE Collaboration, Eur. Phys. J. C **77**, 33 (2017). arXiv:1509.07541
30. B. Abelev, et al., ALICE Collaboration, Eur. Phys. J. C **73**, 2456 (2013). arXiv:1208.4968
31. J. Adam, et al., ALICE Collaboration, Phys. Rev. Lett. **116**, 222302 (2016). arXiv:1512.06104
32. C. Albajar, et al., UA1 Collaboration, Nucl. Phys. B **335**, 261 (1990)
33. J.S. Moreland, J.E. Bernhard, S.A. Bass, Phys. Rev. C **92**, 011901 (2015). arXiv:1412.4708
34. J.E. Bernhard, J.S. Moreland, S.A. Bass, Nucl. Phys. A **967**, 293 (2017). arXiv:1704.04462
35. K.J. Eskola, K. Kajantie, P.V. Ruuskanen, K. Tuominen, Nucl. Phys. B **570**, 379 (2000). arxiv:hep-ph/9909456
36. H. Song, U.W. Heinz, Phys. Rev. C **78**, 024902 (2008). arXiv:0805.1756
37. Z. Qiu, U.W. Heinz, Phys. Rev. C **84**, 024911 (2011). arXiv:1104.0650
38. H. Niemi, G.S. Denicol, H. Holopainen, P. Huovinen, Phys. Rev. C **87**, 054901 (2013). arXiv:1212.1008
39. J. Noronha-Hostler, L. Yan, F.G. Gardim, J.-Y. Ollitrault, Phys. Rev. C **93**, 014909 (2016). arXiv:1511.03896
40. L. Yan, Chin. Phys. C **42**, 042001 (2018). arXiv:1712.04580
41. J. Adam, et al., ALICE Collaboration, Phys. Rev. Lett. **116**, 132302 (2016). arXiv:1602.01119
42. W. Greiner, J.A. Maruhn, *Nucl. Models* (Springer, Berlin, 1996)
43. S. Kamerdzhiev, J. Speth, G. Tertychny, Phys. Rep. **393**, 1 (2004). arxiv:nucl-th/0311058
44. B.G. Zakharov, JETP Lett. **105**, 758 (2017). arXiv:1703.04271
45. B. Schenke, P. Tribedy, R. Venugopalan, Phys. Rev. Lett. **108**, 252301 (2012). arXiv:1202.6646
46. B. Schenke, P. Tribedy, R. Venugopalan, Phys. Rev. C **86**, 034908 (2012). arXiv:1206.6805